npj | clean water

Article

Published in partnership with King Fahd University of Petroleum & Minerals

https://doi.org/10.1038/s41545-024-00306-9

Adsorption and DFT investigations of Cr(VI) removal using nanocrystals decorated with graphene oxide

Simranjeet Singh[1], Amith G. Anil[2], Basavaraju Uppara[2,3], Sushant K. Behera[2], Bidisha Nath[4], Pavithra N[1], Shipra Bhati[5], Joginder Singh[6], Nadeem A. Khan[7] & Praveen C. Ramamurthy[1]

In this research, a solvothermal approach is introduced to synthesize a metal-organic frameworks (MOFs) nanocomposite (GO/UiO-66-NDC) for the removal of Cr(VI) from water. A comprehensive analysis was performed to understand the physical, chemical, and structural properties of the MOF nanocomposite. The adsorption behavior of Cr(VI) was investigated by changing various parameters, such as pH, dosage, and concentration, to determine isotherms, thermodynamics, and kinetics. The results showed that the nanocomposite had a high tolerance to pH and thermal stability, with a high adsorption capacity of 157.23 mg g^{-1} for Cr(VI) at pH 3 due to the presence of zirconium oxide clusters. The density functional theory simulations showed that the nanocomposite had ten times more dynamic delocalized surface states, which enhanced the adsorption capacity and agreed with the experimental results. Furthermore, the nanocomposite exhibited better regeneration performance compared to previously reported materials, making it a promising super-adsorbent for removing Cr(VI) from water.

The most significant cause of water pollution is chemical pollution, such as heavy metal pollution and various synthetic organic chemicals[1,2]. River and stream ecosystem contamination is a growing global concern[3]. Due to the rapid expansion of the heavy metal industry in recent years, heavy metal and pesticide pollution has become a severe health and environmental hazard. These contaminants in high concentrations in the ecosystem harm aquatic and terrestrial organisms[4,5]. They induce accumulative poisoning, severe damage to the neurological system, lung congestion, liver damage, and oedema in humans. Some pollutants are also carcinogenic[6,7].

Chromium (Cr), the first Group 6 element of the periodic table, is the most prevalent heavy metal in groundwater and surface water, and it is frequently derived via chromate manufacturing, metallurgy, metal electroplating, textile dyeing, wood preservation, and tanneries[8,9]. The acceptable limit of hexavalent chromium in water for human consumption, according to the WHO, is 50 μg L^{-1} [10]. However, Cr(VI) ratios in industrial wastewater range from 5 g L^{-1} to 270 mg L^{-1} [11]. These statistics necessitate the need for water treatment for the removal of chromium. Several methods have been proposed for removing chromium, including chemical precipitation, electrochemical processing, ion exchange, membrane filtration, separation, and adsorption[12,13]. Other treatment processes, except adsorption, have substantial downsides, such as expensive pricing, vast volumes of chromium sludge generated, and effective disposal costs[14,15]. Adsorption procedures are practical and cost-effective strategies for eliminating chromium ions from wastewater[16]. These methods are based on the reliable binding of metal ions to the adsorbent material, which is dependent on analyte-sorbent interactions during the adsorption process[17,18]. Metal-organic frameworks (MOFs) are porous inorganic-organic hybrids made up of a regular array of metal ions linked by "linker" molecules (organic)[19,20]. Due to their excellent structural homogeneity, homogenous pore structures, adjustable porosity, extensive variety, and flexibility in geometry, chemical functionality, network size, and topology, they provide distinctive structural diversities when compared to other porous materials[21,22]. UiO-66 framework (University of Oslo) is a 3D porous material with intriguing features that make it a promising material for adsorption research, including large and uniform pore

[1]Interdisciplinary Centre for Water Research (ICWaR) Indian Institute of Science, Bengaluru, Karnataka 560012, India. [2]Department of Materials Engineering, Indian Institute of Science, Bengaluru, Karnataka 560012, India. [3]Centre for Smart Manufacturing Precision Machines (C-SMPM), Central Manufacturing Technology Institute (CMTI), Bengaluru, Karnataka 560022, India. [4]Interdisciplinary Centre for Energy Research (ICER) Indian Institute of Science, Bengaluru, Karnataka 560012, India. [5]Department of Chemistry, The Oxford College of Engineering, Bangalore, India. [6]Department of Botany, Nagaland University, Lumami, Nagaland 798627, India. [7]Interdisciplinary Research Center for Membranes and Water Security, King Fahd University of Petroleum and Minerals, Dhahran 31261, Saudi Arabia. e-mail: onegroupb203@gmail.com

size, excellent hydrothermal and chemical stability, a high surface area, excellent water stability, good biocompatibility, and active clusters of Zr-O[23,24]. The UiO-66-NDC MOF has $Zr_6O_4(OH)_4$ as secondary building blocks that work with twelve bridge ligands, or 1,4-NDC, to create a three-dimensional structure with an octahedral center hole cage and corner cages (eight tetrahedral)[25]. It possesses a strong ZrO bond and coordinatively unsaturated Zr^{4+} sites that help with adsorption and mass transfer[26].

UiO-66 is known for its stability and facile preparation; however, it is impeded by a notable drawback of low adsorption capacity and selectivity, limiting its broad utility[27]. To overcome this limitation, the modification of UiO-66 with specific functional groups emerges as a promising strategy to yield adsorbents characterized by heightened capacity and selectivity[28]. Adhering to the principles of Lewis acid-base (HSAB) theory, certain metal ions exhibit a preferential reactivity with distinct functional ligands such as $-NH_2$, –OH, and –S, facilitated through ion exchange, electrostatic interaction, and chelation mechanisms. Notably, a specific ligand, functioning as a Lewis base, contributes a lone pair electron, establishing a stable coordination bond with heavy metal ions (functioning as Lewis acid). This coordinated interaction facilitates the effective removal of harmful metals, underscoring the potential of UiO-66 modifications for achieving enhanced efficacy in the remediation of heavy metal contaminants. Removal of Cr(VI) using UiO-66 was also investigated and adsorption capacity was found to be 85.6 mg g^{-1} [29].

The modification of UiO-66 with the N-O functional group has also been reported for the removal of Cr(VI), demonstrating a maximum adsorption capacity of 60.24 mg g^{-1} [30]. UiO-66 MOF nanoparticles based on cerium are stable in different types of wastewater, resist protons and hydroxide ions, and eliminate both organic and inorganic pollutants[31]. UiO-66 particles embedded on granular corncob used for Cr(VI) removal exhibit an adsorption capacity of 90.04 mg g^{-1} [32]. The application of UiO-66 modification involving the incorporation of NH_2 functional group has been documented in the context of Cr(VI) removal, revealing a noteworthy maximum adsorption capacity of 32.36 mg g^{-1} [33]. In our literature exploration regarding Zr-MOFs employed as chromium adsorbents, it was observed that, despite their notable stability, they did not exhibit a particularly high adsorption capacity.

Graphene oxide and its composites have been thoroughly investigated as a robust adsorbent material. In addition to having more surface area, functionalized graphene oxide nanocomposites also contain heteroatoms and functional groups that improve interaction with the target ion[16,34,35]. The intercalation of graphene oxide (GO) with UiO-66-NDC further enhances its adsorption performance, creating a synergistic effect. Previous studies have demonstrated the efficacy of UiO-66-NDC in adsorbing various heavy metals, such as Cr(VI), owing to its well-defined pores and strong metal-ligand interactions. Introducing graphene oxide into the composite not only provides additional active sites but also improves the overall stability and conductivity, enhancing the adsorption capacity. This composite material exhibits improved adsorption kinetics and thermodynamics, making it a promising candidate for the efficient removal of Cr(VI) from water systems. The combined advantages of UiO-66-NDC and graphene oxide intercalation offer a versatile and effective solution for addressing heavy metal contamination in aqueous environments.

The present study aims to assess the effectiveness of GO/UiO-66-NDC nanocomposite, which was synthesized by combining the advantages of UiO-66-NDC and graphene oxide nanocomposite to remove Cr(VI). The stated objectives of this work are to (1) synthesize GO/UiO-66-NDC using a solvothermal method and characterize it in detail and (2) ascertain the effects of the GO/UiO-66-NDC nanocomposite on the initial ion concentration, pH, and dose. (3) Information on the removal process (4) Research on adsorption isotherms, thermodynamics, and kinetics to comprehend the adsorption process's nature

Results and discussion

Dynamic nature of the system

A stable configuration of the GO/UiO-66-NDC system with minimum surface energy is simulated with geometry optimization considering Broyden-Fletcher-Goldfarb-Shanno (BFGS) algorithm[36]. Heavy atoms like Zr make the nanocomposite system dynamic over the GO system (Fig. 1a). The total dynamic nature of the GO/UiO-66-NDC system is clearly reflected, affecting the atomic configuration of the supercell. This dynamic stability of the nanocomposite makes it a superior platform to adsorb heavy

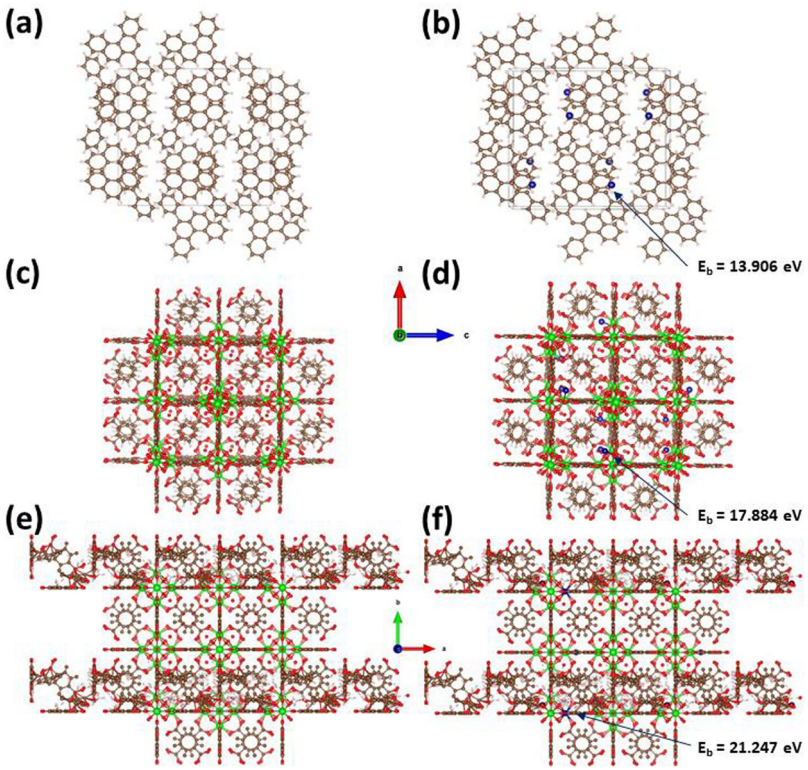

Fig. 1 | Structural optimization and relaxation. Optimized structure of (**a**) graphene oxide (GO), (**b**) GO with Cr (VI) adsorbed on surface, (**c**) UiO-66-NDC, (**d**) UiO-66-NDC with Cr(VI) adsorbed on surface, (**e**) UiO-66-NDC/GO nanocomposite, and (**f**) nanocomposite with Cr(VI) adsorbed on surface. The values of binding energies (E_b) are noted in each case of (**b**, **d**, **f**) for Cr(VI) adsorption.

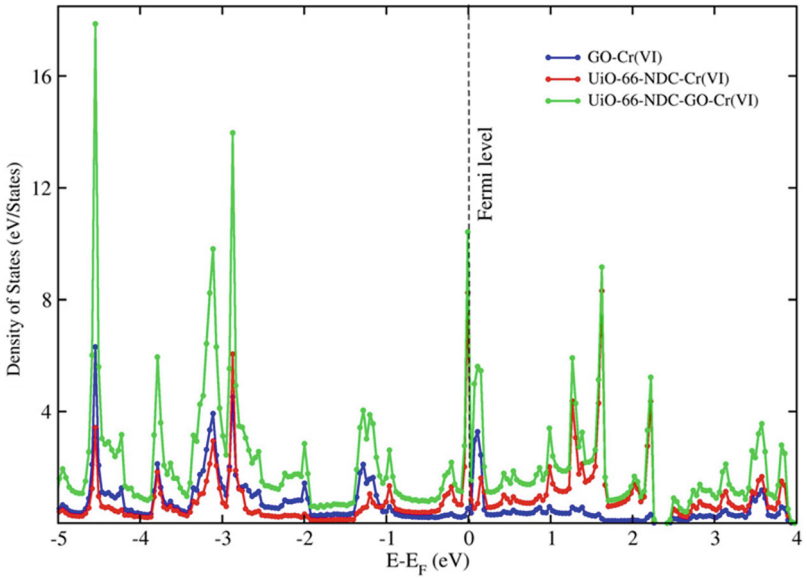

Fig. 2 | Electronic density of states of the optimized systems. Density of states (DOS) plot for all three systems (i.e., GO, UiO-66-NDC and UiO-66-NDC/GO nanocomposite) after Cr(VI) adsorption.

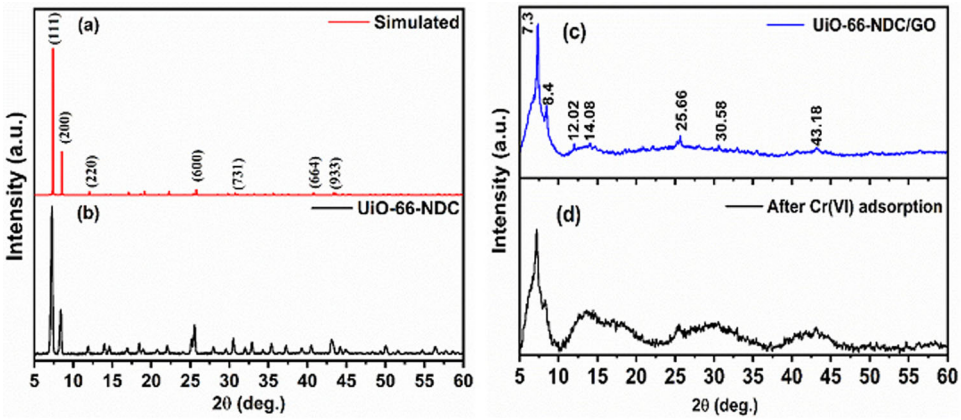

Fig. 3 | Structural parameters of the synthesized materials. PXRD pattern of the (**a**) Simulated UiO-66-NDC, (**b**) Synthesized UiO-66-NDC, (**c**) synthesized GO/UiO-66-NDC nanocomposite and (**d**) after Cr adsorption.

metals. It is obtained that GO achieves close to -179.291 Ry total energy as a unit, whereas GO/UiO-66-NDC clears the mark at -1321.457 Ry total energy in the iteration steps till the optimization process.

Similarly, UiO-66-NDC achieves -321.552 Ry total energy during the optimization process. This energy mark clearly proves that it becomes almost 10 and 4 times more dynamic than pristine GO systems and UiO-66-NDC, respectively. The delocalized Zr atoms on the nanocomposite surface (Fig. 1b) are responsible for the increase in total energy, which suggests that, unlike the GO system, all Zr atoms delocalize on the surface. The carbon atom in the GO system only exists in localized states, which results in a lower overall energy without any dynamic properties for adsorption. In pristine UiO-66-NDC (Fig. 1c), the Zr atoms are localized and stay in a confined energy domain, like Cr(VI) atom adsorptions (Fig. 1d). As a result, the dynamic behavior is controlled and stable.

It is observed that the value of E_b is increasing gradually from pristine GO to UiO-66-NDC and then in the UiO-66-NDC/GO nanocomposite system (Fig. 1e). This trend reflects the efficient adsorption of the Cr(VI) metal on the nanocomposite surface (Fig. 1f). Considering the density of states (DOS) plots, it is noticed that the UiO-66-NDC/GO nanocomposite system is more dynamic compared to both pristine parent systems (i.e., GO and UiO-66-NDC) while the Cr(VI) adsorbed on the respective surfaces (Fig. 2). It is happening due to the phase transformation from localized state in pristine (i.e., GO, UiO-66-NDC and nanocomposite) to delocalized states after metal adsorption that checks the suitability of the nanocomposite system to adsorb Cr(VI) metal. Besides, the Zr atoms get delocalized on the surface of the UiO-66-NDC/GO nanocomposite system making the nanocomposite dynamic for Cr(VI) adsorption studies, strongly supporting the experimental results.

Meanwhile, the nanocomposite bears GO, and the presence of GO makes the Zr atoms delocalize over the nanocomposite surface, leading to an enhancement in energy values. That is the sole reason for the improvement in the dynamic behavior of nanocomposite compared to both pristine GO and UiO-66-NDC components. In contrast to the localized surface states of carbon in the graphene oxide system, Zr-based delocalized surface states are now taking center stage in the GO/UiO-66-NDC nanocomposite system. This type of phase transformation from the localized state in GO and UiO-66-NDC pristine form to delocalized states in GO/UiO-66-NDC nanocomposite makes the nanocomposite system a relevant surface to adsorb metals having compatible work functions like Zr. This makes the nanocomposite surface adsorption active for heavy metals like Chromium (Cr). In order to support the experimental findings, Cr adsorption studies show that Zr atoms become delocalized along the surface of the GO/UiO-66-NDC nanocomposite, making the nanocomposite dynamic (10 times compared to the pristine GO system and 4 times compared to the pristine UiO-66-NDC system).

Material characterizations

Figure 3a illustrates the powder XRD patterns of as-synthesized UiO-66-NDC, which are strikingly similar to the simulated powder XRD pattern of UiO-66-NDC (Fig. 3b). Strong diffraction peaks at 7.3° and 8.4° show that the crystalline structure of UiO-66-NDC and UiO-66 are identical[37].

Table 1 | Supporting structural parameters of simulation for UiO-66-NDC MOF

Atom	x	y	z	Displacement (Å^2)	Occupancy Factor	Atoms/Unit Cell
C	0.14112	0	−0.14112	0.002	1	48
C	0.19088	0	0.19088	0.042	1	48
C	0.25202	0.02802	0.18864	0.022	0.5	96
C	0.26611	0.05612	0.12921	0.141	0.25	48
C	0.32274	0.08422	0.11692	0.352	0.25	48
O	0.15881	0	0.08942	0.044	1	96
O	0.05574	−0.05574	−0.05574	0.023	1	32
Zr	0.10778	0	0	0.011	1	24

Figure 1c shows the UiO-66-NDC MOF's optimized structure as determined by DFT modeling. VESTA software is utilized to obtain the simulated PXRD pattern for this improved UiO-66-NDC MOF in order to compare the simulated and experimental UiO-66-NDC. The structural parameters are summarized below in Table 1 and Supplementary Table 1, which has been obtained from simulation and compared with experimental PXRD data. When compared to experimental PXRD data, which is almost identical with a 0.04% variation, it was found that simulation results varied by 0.04%. This demonstrates how the simulation data substantially supports the PXRD data from the experiment and verifies the MOF's structural stability and successful MOF production.

For the UiO-66-NDC MOF in the Fm-3m space group (Number 225), the following structural parameters were retrieved from the DFT simulation: (x, y, z); fractional coordinates; atomic displacement factors during optimization; atomic occupancy factors; and the number of atoms in the unit cell. The simulation cell volume, $V = 8919.45443$, and the lattice cell parameter are both equal to 20.7386. For improved convergence, the occupancy factors of all atoms have been set to units.

Additionally, XRD data for the UiO-66-NDC/GO nanocomposite were gathered both before and after Cr(VI) adsorption. The diffraction patterns at 7.3° and 8.4° are ascribed to typical patterns of UiO-66-NDC, as illustrated in Fig. 3b. The diffraction patterns at 7.3° and 8.4° are ascribed to typical patterns of UiO-66-NDC, as illustrated in Fig. 3c. The intensity of these two peaks was significantly reduced after Cr(VI) adsorption. Additional extremely faint patterns (at 12.02°, 14.08°, 25.24°, 25.66, 30.58, 40.56, 43.18, etc.) were also totally eliminated (Fig. 3d). This wide peak demonstrates the material's amorphous nature. This indicates that the Cr(VI) adsorption on the MOF has significantly reduced the crystallinity. It implies that when absorbing Cr, the UiO-66-NDC/GO experiences a structural alteration (VI).

Raman investigations provide further proof of the GO-doped UiO-66-NDC nanocomposite material. The vibrational frequencies for both pure and Cr(VI) adsorbed nanocomposite materials are presented in Fig. 4a. An intense Raman peak at 1585 cm^{-1} is ascribed to the NDC linker's CC aromatic stretching vibration[38], and the weak peak at 664 cm^{-1} is attributed to aromatic-ring in-plane bending vibration[39]. The doublet peaks at 1454 cm^{-1} and 1425 cm^{-1} are due to in-phase O=C=O symmetric stretching vibrations of the carboxylate group in the NDC linker[39]. The peaks at 1516 cm^{-1} and 1356 cm^{-1} are ascribed to in-plane ring deformation[39], and the sharp peak at 776 cm^{-1} is ascribed to out-of-plane C−H asymmetric bending vibration of NDC linker[40]. These vibrational frequencies match UiO-66-NDC material[41,42]. However, the vibrational frequencies for GO, which appear around 1350 cm^{-1} and 1585 cm^{-1} [43], are submerged under the vibrational frequencies of the NDC linker and are similar to the previous findings[3,44]. Similar peak locations have been reported in pristine and Cr(VI) adsorbed GO/UiO-66-NDC. The Raman active peaks may not impact the adsorbent as a result. In FTIR analysis, this is further and clearly defined[45].

As seen in Fig. 4b, the two strong absorption peaks at 353 nm and 264 nm of the UV spectrum for GO/UiO-66-NDC nanocomposite were noted. The absorption peak centered at 353 nm arises from the π- π* transition of naphthalene rings, whereas the other peak at 264 nm is characteristic of the graphene oxide π–π* transition[3,45]. The observed peaks before the experiment are in line with the previous studies[3,44]. The absorption spectra change significantly after the uptake of Cr(VI) ions. Two new absorptions are observed around 439 nm and 605 nm. The red shift in π–π* absorption arises from the doping of GO with chromate ions. Adsorption of chromate ions increases the concentration of π electrons, resulting in a red-shifted absorption. The graphene oxide absorption shows a redshift, and the intensity of naphthalene ring absorption reduces notably along with a slight redshift. These changes ascertain to Cr(VI) binding onto the adsorbent matrix.

The functional group characterization of GO/UiO-66-NDC nanocomposite was carried out using FTIR-ATR mode. FTIR spectra of GO/UiO-66-NDC nanocomposite were recorded before and after the adsorption of Cr(VI), as shown in Fig. 4c. In pristine nanocomposite, the faint peak at 3617 cm^{-1} and broad peak centered at 3355 cm^{-1} are attributed to -OH stretching vibration of unperturbed $Zr_6O_4(OH)_4$ cluster and NDC linker, respectively[41]. The peak at 1557 cm^{-1} is attributed to the asymmetric stretching of the carboxylate group. The sharp peaks at 1365 and 1415 cm^{-1} are assigned to out-of-phase O=C=O stretching vibration of the carboxylate group and C-C stretching and C-H bending vibrations of the NDC linker, respectively. The sharp peaks at 650, 785 and 1263 cm^{-1} are attributed to symmetric bending vibration, out-of-plane asymmetric and of C-H of NDC linker and C=C stretching vibration. The peaks before adsorption are concurrent with the previous studies[3,44]. FTIR studies of Cr(VI) adsorption show that the -OH peaks were completely diminished after adsorption. Strikingly, the antisymmetric COO^- stretching at 1557 cm^{-1} shows shifting to 1568 after Cr(VI) adsorption, possibly due to the interaction with the chromate ion. The FTIR results represent that the -OH and COO groups in the nanocomposite play an important part in the adsorption of Cr(VI).

As shown in Fig. 4d, the results of a TGA performed by a TGA analyzer (TA Q50) in an ambient environment at a ramp rate of 10 °C min/min are presented. According to the TGA thermogram, two considerable weight reductions were observed. A loss of 11.26% was noticed between 20 and 110 °C, which may be ascribed to the escape of moisture and solvent molecules from the dimethyl formamide that was kept in the material's porous network. From 110 to 600 °C, a further weight loss of 41.04% was seen, which is consistent with the earlier results and is caused by the organic linker (1,4-naphthalene dicarboxylic acid) decomposing[46].

The XPS spectra were recorded within the 0–1300 eV range to elucidate the binding energies associated with the synthesized material GO/UiO-66-NDC before (Fig. 5a) and after Cr(VI) adsorption (Fig. 5b). In Fig. 5a, the distinctive binding energies of Carbon (C), Zirconium (Zr), and Oxygen (O) are illustrated. Peaks corresponding to the 1s orbitals of oxygen and carbon, as well as the 3d orbital of zirconium, indicate the presence of these elements in the GO/UiO-66-NDC. Following adsorption, the emergence of a new peak in the Cr2p spectrum confirms the successful adsorption of chromium on the GO/UiO-66-NDC. Specifically, the spectral peaks at 288.1 and 283.9 eV can be attributed to the O-C=O and C=C bonds, respectively (Fig. 5c). The deconvolution of the Zr 3d spectra revealed two peaks at 184.7 and 182.8 eV, corresponding to the Zr $3d_{3/2}$ and Zr $3d_{5/2}$ related to Zr–O bond of zirconium (Fig. 5e). Further deconvolution of the O 1 s spectrum resulted in a peak at

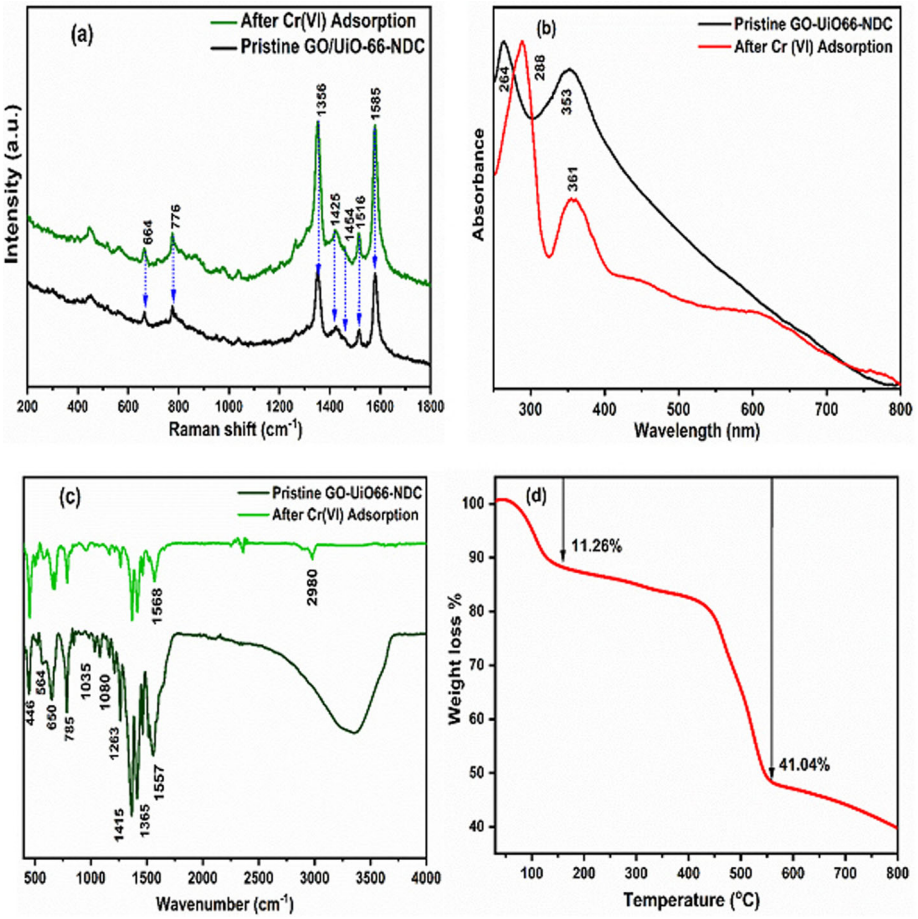

Fig. 4 | Structural and optical analysis of synthesized materials. a Raman spectrum of the synthesized GO/UiO-66-NDC and after Cr(VI) adsorption, (**b**) UV studies of the pristine GO/UiO-66-NDC and after Cr(VI) adsorption, (**c**) GO/UiO-66-NDC nanocomposite FTIR spectra before and after the experiment, (**d**) TGA of the synthesized GO/UiO-66-NDC nanocomposite.

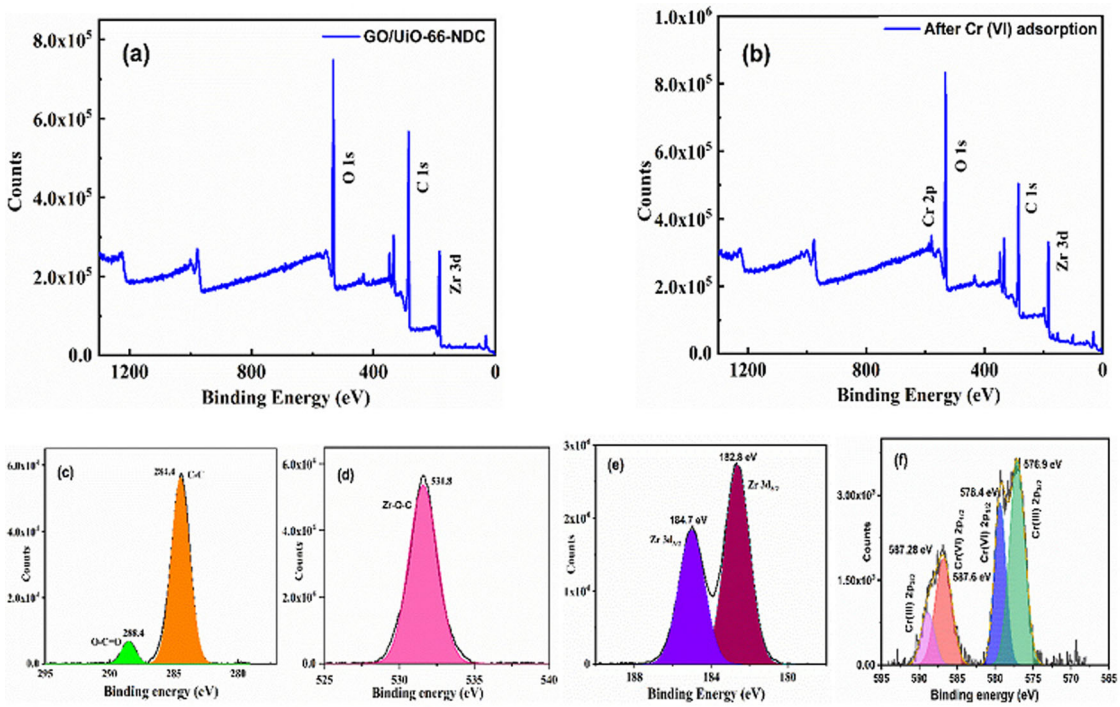

Fig. 5 | XPS analysis of GO/UiO-66-NDC before and after Cr (VI) adsorption. a Survey scan of GO/UiO-66-NDC (**b**) Survey scan of GO/UiO-66-NDC after Cr(VI) adsorption, (**c**) carbon (**d**) oxygen, (**e**) Zirconium and (**f**) Cr 2p after Cr adsorption.

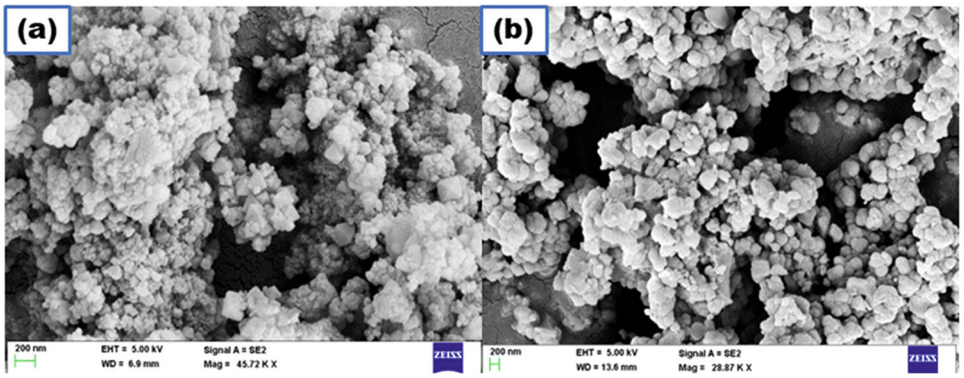

Fig. 6 | SEM/EDX micrographs of the synthesized GO/UiO-66-NDC nanocomposite. a before and (**b**) after Cr(VI) adsorption.

531.8 eV, indicative of the Zr–OH bond (Fig. 5d). After Cr(VI) adsorption, two distinct peaks at 576.9 eV ($2p_{3/2}$), 587.28 eV ($2p_{3/2}$), attributed to Cr (III) and peak position at 587.6 eV ($2p_{1/2}$) and 578.4 eV($2p_{1/2}$) corresponds to Cr(VI) (Fig. 5f)[47]. These findings suggest that, under acidic conditions, a fraction of Cr(VI) underwent reduction to Cr (III) subsequent to its adsorption by GO/UiO-66-NDC. The preceding findings distinctly indicate the successful occurrence of ion exchange in the adsorption process.

The morphology and surface elemental composition of the synthesized materials were examined by SEM and EDX respectively. As shown in Fig. 6, the GO/UiO-66-NDC nanocomposites have a highly porous structure. The structure resembles microporous structures in that it is made up of multiple asymmetric nanoparticles that have been fused together. The morphology also includes a number of big, sharp-edged crystals, which is consistent with the XRD results. A study conducted by EDS indicated that the nanocomposite is mainly comprised of zirconium, carbon, and oxygen (Table 2). The SEM and EDS investigations were also carried out after the adsorption tests. The micrograph shows a discernible alteration in surface morphology following adsorption experiments. Cr particles embedding on the surface cause the surface to seem less porous with smoother edges. The effective incorporation of Cr into the nanocomposite matrix is further confirmed by EDS analysis.

Adsorption of Cr (VI) onto GO/UiO-66-NDC

Figure 7a shows the pHpzc value on the surface of GO/UiO-66-NDC nanocomposite, which was 5.32. In contrast, the anion form of chromium ($HCrO_4^-$) adsorption is more favorable at pH values below pHpzc[48]. This implies that at pH values less than 5.32, Cr(VI) adsorption is highly favorable, which could be due to significant electrostatic attraction between the protonated oxygen and anion ($HCrO_4^-$) containing functional groups situated on the GO/UiO-66-NDC nanocomposite surface. The surface of the GO/UiO-66-NDC attracts the negatively charged chromate ions at pH < point of zero charges by electrostatic interaction. For pH > PzC, the surface of GO/UiO-66-NDC becomes negatively charged, which hinders the removal of Cr(VI) due to competition with hydroxyl ions and electrostatic repulsion[49]. Our GO/UiO-66-NDC nanocomposite results are consistent with the findings of other researchers who found that adsorption for Cr(VI) is higher at low pH[50].

Figure 7b shows the results of determining the impact of pH on the adsorption of Cr(VI) by GO/UiO-66-NDC nanocomposite at pH values ranging from 2 to 12. The process of Cr(VI) adsorption increased from pH 2 to 3 and then began to decline after that point. The findings show that at pH 3, 10 mg L^{-1} of starting Cr(VI) concentration at a dosage of 0.5 g L^{-1} resulted in the highest removal capacity of 75.61%. From pH 3 to 12, the adsorption capacity diminishes as the pH rises. This shows that the pH of the solution affects the interaction between chromium speciation and adsorbent surface charge.

In the solution, Cr(VI) ions exist in several forms, i.e., dichromate ($Cr_2O_7^{2-}$), chromate (CrO_4^{2-}), and hydrogen chromate ($HCrO^{4-}$) ions. The presence of these chromium ions depends on the total chromate concentration, solution pH, and redox potential[51]. It was revealed that raising the pH above 3 resulted in decreased Cr(VI) adsorption, but lowering the pH significantly enhanced Cr(VI) adsorption. The adsorbent material functioned better in acidic than neutral or alkaline environments, with a maximum adsorption capacity attained at pH 3.0. Between pH 1–2, the chromium ion exists in the form of H_2CrO_4, while in the range pH 2.0-3.0 Cr(VI) is predominantly found as negatively charged hydrogen chromate ($HCrO_4^-$) ions, and between pH range 4.0–12.0 chromate ions (CrO_4^{2-}) are prevalent[52]. The point of zero charge determination study revealed that the pHpzc value for GO/UiO-66-NDC nanocomposite was 5.32. The surface charge of GO/UiO-66-NDC nanocomposite was positive when the pH was <5.32, while it was negative when pH > 5.32. Therefore, the positively charged surface of the GO/UiO-66-NDC nanocomposite adsorbent is attracted to negatively charged Cr(VI) species ($HCrO_4$) at pH 3 levels as shown in Eq. 1, and the adsorption mechanism was attraction via electrostatic. Nevertheless, at a pH lower than 3.0, a reduction in adsorption was noted, attributable to the presence of H_2CrO_4 ions. A pronounced competition emerged between H_2CrO_4 and protons for available adsorption sites. Conversely, at higher pH levels, specifically within the range of 4.0 to 12.0, the prevailing chromium species is CrO_4^{2-}. Elevated concentrations of OH- ions in the chromium solution engage in a competitive relationship with chromate (CrO_4^{2-}) ions for adsorption onto the adsorbent surface (Eq. 2), with OH- ions exerting a predominant influence. Consequently, the adsorption capacity of Cr(VI) diminishes with an increase in pH. Given that the maximum adsorption capacity of Cr(VI) was observed at pH 3, this pH value was chosen as the optimal condition for the various experiments. The present studies are consistent with the previous findings, which showed a similar tendency with maximum adsorption capacity at low pH[53].

$$R^+ \xrightarrow{HCrO_4^-} R[HCrO_4^-]n \quad (1)$$

$$R^+ \xrightarrow{CrO_4^{-2}} R[CrO_4^{-2}]n \quad (2)$$

Where R and n represent the skeleton of GO/UiO-66-NDC nanocomposite and a number of the ions adsorbed on the surface, respectively. Entezari

Table 2 | Illustration of Energy Dispersive Spectroscopic (EDS) analysis of GO/UiO-66-NDC nanocomposite (a) before and (b) after the adsorption of hexavalent chromium

Before Adsorption			After Cr (VI) adsorption		
Element	Weight %	Atomic %	Element	Weight %	Atomic %
C K	49.61	70.88	C K	53.04	69.01
O K	20.98	23.32	O K	27.93	27.28
Zr L	29.41	5.80	Cr K	3.40	1.02
			Zr L	15.63	2.68
Totals	100.00		Totals	100.00	

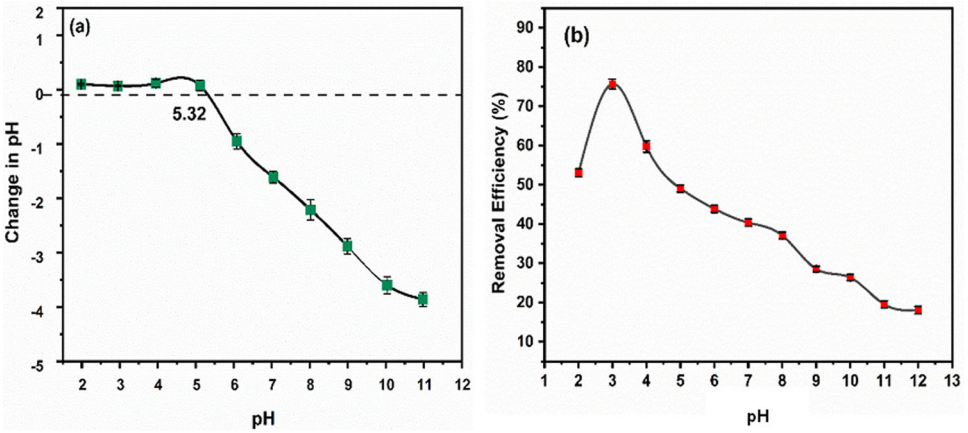

Fig. 7 | Influence of point of zero charge and pH on the nanocomposite surface. a Determination of zero-point charge (pHpzc) on GO/UiO-66-NDC Nanocomposite surface, (**b**) Effect of pH of Cr(VI) on the adsorption onto GO/UiO-66-NDC nanocomposite. $T = 25$ °C, $V = 100$ mL, Dose 50 mg, Ion rate = 10 mg L^{-1}. Error bars represent the standard deviations.

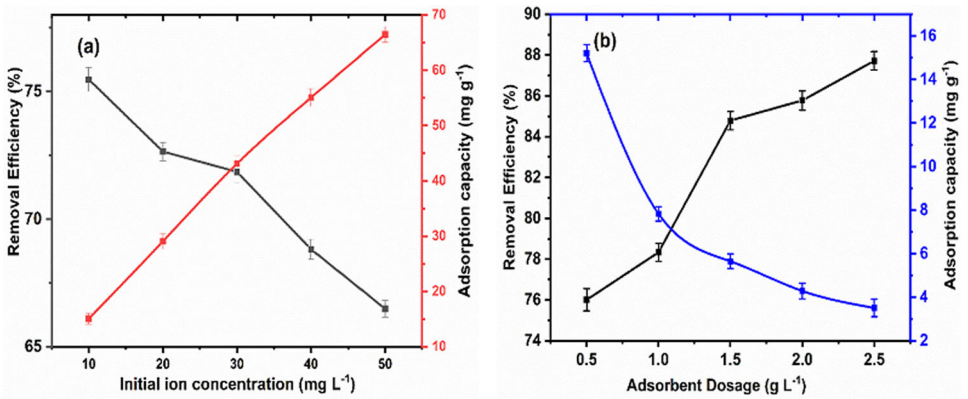

Fig. 8 | Effect of different parameters on Cr(VI) adsorption of nanocomposite. a The optimal level of Cr(VI) for the elimination of Cr(VI) onto GO/UiO-66-NDC nanocomposite. $T = 25$ °C, $V = 100$ mL, pH = 3, Ion rate = 10 mg L^{-1}, (**b**) Impact of the beginning ion rate on the Cr(VI) adsorption onto GO/UiO-66-NDC nanocomposite. $T = 25$ °C, $V = 100$ mL, pH = 3, $m = 50$ mg. Error bars represent the standard deviations.

et al.[54] attributed the high capacity for chromium adsorption at acidic pH to the presence of various forms of Cr(VI) in the solution, including $HCrO_4^-$, CrO_4^{2-}, H_2CrO_4, and $Cr_2O_7^{2-}$[54]. In a study by ref. 55. CTAB/H_2O_2- clay was utilized for chromium removal, with the results indicating the highest adsorption capacity at a pH of approximately 2[55].

The relationship between the dosage of GO/UiO-66-NDC nanocomposite removal efficiency and the adsorption capacity of Cr(VI) is represented in Fig. 8a. The effect of dose on Cr(VI) adsorption was determined by shaking a series of 100 mL of Cr(VI) 10 mg L^{-1} with initial pH of 3.0 for 150 min at 298 K. The number of adsorbents in these solutions ranged from 0.5 to 2.5 g L^{-1}. The removal percentage of Cr(VI) increased remarkably with the increment in dosage from 0.5 g L^{-1} to 2.5 g L^{-1}. It was observed that with the increment in dosage from 0.5 g L^{-1} to 2.5 g L^{-1}, the removal efficiency increases from 76.01% to 87.71%, while the equilibrium adsorption capacity decreases from 15.20 mg/g to 3.50 mg/g. This may be explained as follows: Increased adsorbent dose may result in increased contact surface area and accessible adsorption active sites, resulting in maximal Cr(VI) removal. The percentage removal reaches 87.71% at 2.5 g L^{-1}. The elimination rate is unaffected by additional dosage increases since more GO/UiO-66-NDC vacant sites are being created at the same time. High dosages of the adsorbent lead to aggregation, which reduces the amount of Cr(VI) that can be absorbed. This eventually decreases the unit contact area between Cr(VI) ions & GO/UiO-66-NDC adsorption capacity decreases[56]. At a dosage exceeding the optimum level, the adsorption capacity of the adsorbent remained nearly constant upon further increases in dosage. This phenomenon may be attributed to the overlapping or aggregation of adsorption sites on the adsorbents, resulting in a reduction of the total surface area. The outcomes of this investigation align with the observations of other researchers. Reference 55 findings indicated that as the dosage increases, adsorption efficiency rises due to the incorporation of additional sorption sites[55]. Nevertheless, the augmentation of dosage does not exert any discernible effect on adsorption efficiency.

Cr(VI) ions were used in Fig. 8b to assess the impact of Cr(VI) ions on adsorption using GO/UiO-66-NDC. Upon increasing the initial level of Cr(VI), the equilibrium adsorption rate climbed from 15.09 to 66.48 mg g^{-1}, while the clearance percentage decreased from 75.47% to 66.48%. The nanocomposite's surface is porous and has many sites due to its GO/UiO-66-NDC composition. Cr(VI) was removed from 10 mg L^{-1} in 120 min with a removal rate of 75.47%. After 120 to 150 min, the GO/UiO-66-NDC nanocomposite reached equilibrium in its adsorption capacity. At lower concentrations, chromium molecules exhibit rapid adsorption on the surfaces of GO/UiO-66-NDC. However, as the initial chromium concentration increases, the adsorbent surfaces gradually reach saturation. Ultimately, a decline in adsorption occurs due to the repulsion between chromium molecules. Further increases in ion concentration did not result in a significant change in adsorption[57,58]. According to Wu et al.[33], this may be caused by a decline in some active sites and a weakening of the driving force[33].

Adsorption kinetics is a critical technique for measuring how effectively compounds are adsorbed and investigating the adsorption rate. The experimental data was analyzed using five models of pseudo-second-order kinetics and pseudo-first-order kinetics. The data was best fitted using pseudo-order kinetics using Eqs. 3 and 4. (types 2 and 3). In contrast to Type 3, the Type 2 PSOK graph was plotted between 1/t and 1/qe. The many data parameters are all reported, including the rate constant, experimental and observed calculations, and the equilibrium Cr(VI) adsorbed amount. Figure 9 illustrates the type 2 fitting information. This implies that the chemisorption of electrons shared or exchanged between Cr(VI) ions and GO/UiO-66-NDC can control the adsorption rate. Therefore, it can be inferred that the rate-limiting step in adsorption predominantly involves chemisorption, characterized by valence forces. This likely occurs through

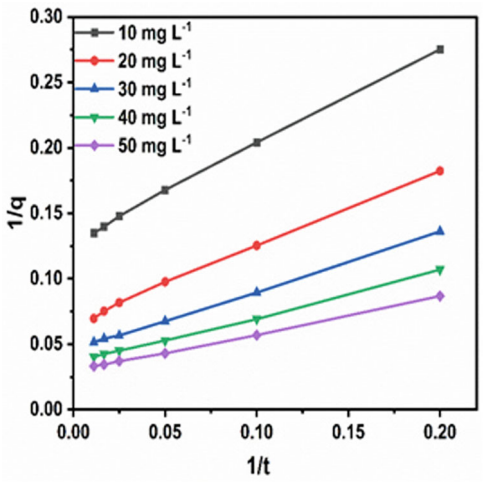

Fig. 9 | Kinetics analysis. Pseudo-second-order kinetics (Type 2) of Cr(VI) on GO/UiO-66-NDC nanocomposite.

the exchange of electrons between chromium and the GO/UiO-66-NDC[59]. Kinetics factors are depicted in Table 3.

By comparing the different models used in this study, the R^2 of both the models were comparatively high compared to other pseudo-order first kinetics. Other parameters for different models are represented in the supplementary section of the MS.

$$\frac{1}{q} = \left(\frac{1}{K_2 q_e^2}\right)\frac{1}{t} + \frac{1}{q_e} \tag{3}$$

$$\frac{1}{t} = \frac{K_2 q_e^2}{q} - \frac{K_2 q_e^2}{q_e} \tag{4}$$

Furthermore, when examining the characteristics of the adsorption process, it has been demonstrated that the crucial step involves determining the adsorption isotherms. According to data presented in Fig. 10 and isotherm parameters in Supplementary Table 2, Temkin, Langmuir, and Freundlich fitted Cr (VI) levels and Cr(VI) adsorbed when equilibrium was reached. Langmuir isotherms are better fitted to the data than Freundlich and Temkin's isotherms, showing that Cr(VI) adsorption onto GO/UiO-66-NDC nanocomposite proceeds via monolayer adsorption. Among the three models, their correlation coefficients show a significant difference. Based on Langmuir fitting, the average q_{max} of the Cr(VI) nanocomposite GO/UiO-66-NDC is 157.23 mg g^{-1}. Monolayer adsorption occurs concurrently with non-uniform surfaces during adsorption. The findings suggest that the Cr(VI) adsorption process on GO/UiO-66-NDC tends to follow monolayer adsorption. The adsorption capacity of Cr(VI) is intricately linked to both the number of available adsorption sites and the specific surface area of the adsorbent[2,22,60–65].

An important factor in determining whether a process will continue favorably or not is thermodynamics (Fig. 11). In order to determine the heat of the adsorption process, it is necessary to examine the relationship between adsorption capacity and adsorption temperature. Based on Eqs. (5, 6, and 7), two quantities can be calculated: enthalpy (*H*), entropy (*S*), and Gibbs energy (*G*):

$$K_{d=\frac{q_e}{C_e}} \tag{5}$$

$$ln\, lnK_d = \frac{\Delta H}{R} - \frac{\Delta H}{RT} \tag{6}$$

$$\Delta G = \Delta H - T\Delta S \tag{7}$$

The graph between *1/T* vs *lnK* for the Cr(VI) adsorption at 298.15, 303.15, 313.15 and 318.15 was plotted to estimate the thermodynamic constant for the GO/UiO-66-NDC nanocomposite, as given in Supplementary Table 3.

GO/UiO-66-NDC Nanocomposite exhibits negative values of G, indicating spontaneous adsorption of Cr(VI). GO/UiO-66-NDC nanocomposite shows positive S values, indicating that the adsorption of Cr(VI) is unpredictable at the solid-solution interface. GO/UiO-66-NDC nanocomposite exhibits endothermic adsorption of Cr(VI).

Table 3 | Pseudo 2nd order kinetics (Type 2) for Cr(VI) adsorption onto GO/UiO-66-NDC nanocomposite

Initial ion	q_e (Experimental value)	Type 2 Pseudo 2nd order kinetics (1/q vs 1/t)		Type 3 Pseudo 2nd order kinetics (1/t vs 1/q)	
		q_e (Theoretical)	R^2	q_e (Theoretical)	R^2
10 mg L^{-1}	7.54	7. 80	0.997	7.80	0.974
20 mg L^{-1}	14.53	15.26	0.994	15.27	0.978
30 mg L^{-1}	21.55	21.92	0.996	21.93	0.99
40 mg L^{-1}	27.53	27.70	0.999	27.71	0.997
50 mg L^{-1}	33.24	33.78	0.996	33.85	0.994

Comparison of the current study findings with previous findings

To demonstrate the feasibility of the created nanocomposite as superadsorbents for Cr(VI) removal, the adsorption capacity of the GO/UiO-66-NDC nanocomposite on Cr(VI) was compared to the effectiveness of other MOFs and nanocomposites found in other papers with similar batch adsorption investigations. The Cr(VI) elimination capacity (mg g^{-1}), at maximum Cr(VI) concentration and employed pH, is summarized in Table 4 (mg L^{-1}) for several adsorbents tested in this work and others. According to the comparison, the nanocomposite described in this paper is a potential adsorbent for extracting Cr(VI) from wastewater.

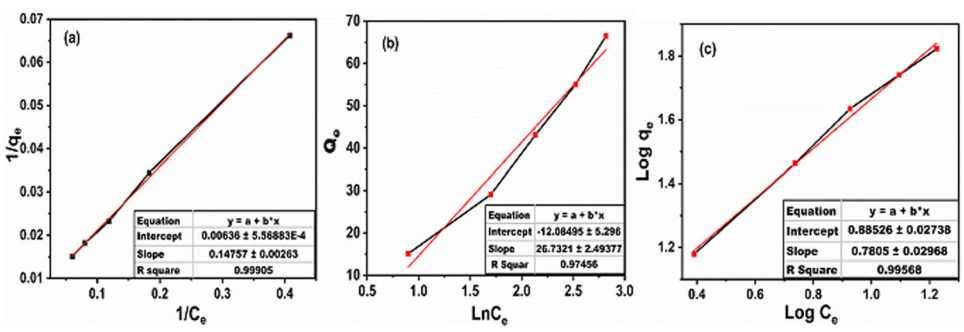

Fig. 10 | Adsorption isotherms. a Langmuir, (**b**) Temkin, and (**c**) Freundlich equations were used to investigate Cr(VI) adsorption on GO/UiO-66-NDC nanocomposite.

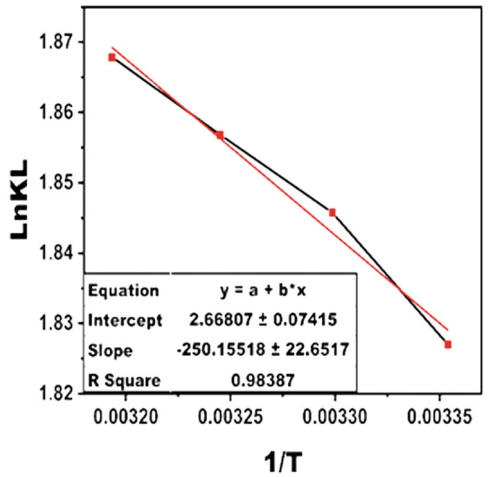

Fig. 11 | Thermodynamic characteristics. Effect of temperature of Cr(VI) adsorption on GO/UiO-66-NDC nanocomposite.

Regeneration studies

Nitric acid of 0.1 M concentration was used in regeneration tests of GO/UiO-66-NDC to recover the adsorbed Cr(VI). Following Cr(VI) adsorption, the GO/UiO-66-NDC was eluted with nitric acid (0.1 M). Figure 12 shows that the removal rate dramatically dropped to 71.23% after six regeneration trials from a higher initial removal rate of 96.4%. The ion exchange contact is what causes the desorption event, and the nanocomposite's functional groups make it easy to regenerate with the acid solution.

In summary, an adsorbent was developed by intercalating the properties of graphene oxide and UiO-66-NDC and employed to adsorb Cr (VI) using batch mode studies. Nanocomposite UiO-66 was functionalized with NDC and graphene oxide. UiO-66 nanocomposites can adsorb 157.23 mg g^{-1} of Cr (VI) despite their substantial area of contact. Compared with other synthetic and industrial adsorbents, this has the most elevated Cr(VI) adsorption capacity. Due to its porous structure with zirconium oxide clusters, GO/UiO-66-NDC has a superior adsorption capacity than other typical nanoparticle adsorbents. With delocalized surface states, the nanocomposite structure is around 10 times more dynamic, giving it an appropriate platform for adsorbing heavy metals like Cr. One of the highest Cr(VI) adsorption capabilities (mg g^{-1}) recorded is represented by the synthesized adsorbent. Additionally, we showed that the nanocomposite had more regeneration cycles than what was previously known. Therefore, GO/UiO-66-NDC performs much better in terms of reusability than previously published findings. GO/UiO-66-NDC nanocomposite may be a potential advanced technology for removing Cr (VI) from industries due to its high adsorption percentage and regeneration capability.

Methods

Chemicals

Potassium dichromate, Graphite (>200 μm), potassium permanganate, Zirconium chloride, and 1,4-naphthalene dicarboxylic acid were of analytical grade>99% procured from Loba Chemie Pvt. Ltd. Bangalore (KA). Solvents like dimethylformamide, ethanol, tetrahydrofuran, sulfuric acid, hydrogen peroxide and hydrochloric acid were obtained from Merck (KA, India).

Synthesis of GO/UiO-66-NDC Nanocomposite

Graphene oxide was synthesized by following the modified Hummers method. For the enhanced procedure, $KMnO_4$ (18.0 g, equivalent to 6 times the weight) was gradually introduced in six equal portions to a 9:1 concentrated H_2SO_4/H_3PO_4 (360:40 mL) and graphite flakes (3.0 g, equivalent to 1 weight unit). This process generated a slight exothermic reaction, carefully monitored to ensure it did not exceed 35–40 °C. Following this, the reaction mixture underwent heating to 50 °C and continuous stirring for a period of 12 h. Subsequently, after completion, the mixture was cooled to room temperature and poured onto ice (approximately 400 mL) containing 30% H_2O_2 (3 mL). The ensuing steps involved sieving the mixture, followed by filtration through polyester fiber. The filtrate then underwent centrifugation at 4000 rpm for 4 h, and the supernatant was meticulously decanted. The remaining solid underwent a sequence of washes with 200 mL of each water, 30% HCl, and ethanol (twice for each). After each wash, the mixture was sifted through a U.S. Standard testing sieve and filtered through polyester fiber, with the filtrate subjected to centrifugation (4000 rpm for 15 min) and subsequent decantation of the supernatant. Following this thorough multiple-wash procedure, the remaining material was coagulated with 200 mL of ether, and the resulting suspension was filtered through a PTFE membrane with a pore size of 0.45 μm. The collected solid on the filter was subjected to overnight vacuum drying at room temperature and was subsequently utilized in the synthesis of the nanocomposite. For GO/UiO-66-NDC nanocomposite, 0.5 wt.% of GO was dispersed in dimethylformamide (150 mL) and sonicated for 8 h. 0.005 mol of $ZrCl_4$ was added to each GO solution and mixed overnight. The mixture was agitated until 1,4-naphthalene dicarboxylic acid (0.005 mol) was entirely dissolved.

Table 4 | Comparison of different studies for Cr (VI) removal using different MOFs and nanocomposites

Materials	Composition	Adsorption capacity Cr(VI)/ $K_2Cr_2O_7$ (mg g^{-1})	pH	Temperature	References
Zr-BDC-$(NH_2)_2$	Zr-MOF, Double amino groups, UiO-66	146	3	303	22
UiO-66-NH_2@ algenic acid	UiO-66, alginic acid	135	~ 3	-	61
UiO-66-NH_2@silica	Zr carboxylate MOF and silica gel	133.4	5	-	23
UiO-66-NH_2(MOR-1)	$[Zr_6O_4(OH)_4(NH_3^+$-BDC$)_6]Cl_6$MOR	119	2	-	62
UiO-66		62	2	-	62
SLUG-21	π -π stacked Ag-bipy chains and 1,2 ethane disulfonate anions	26.9	-	-	63
ZnO-GO	GO and ZnO	8.17	8.2	298	64
CaO-GO	CaO, Graphene oxide	38.04	3	298	65
UiO-66	UiO-66	85.6	7	298	29
UiO-66-NH_2	UiO-66, NH_2	32.36	6.5	298	33
UiO-66 corncob	Corncob, UiO-66	90.04	4–6	298	32
GO/UiO66-NDC	GO, NDC, $ZrCl_4$	157.23	3	298	This work

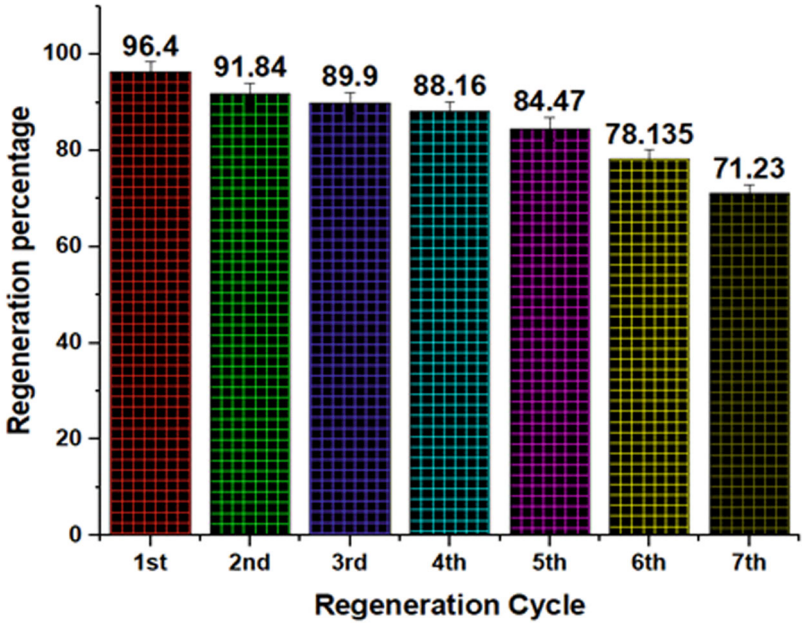

Fig. 12 | Reusability and stability of synthesized GO/UiO-66-NDC nanocomposite. Reusability of GO/UiO-66-NDC for the adsorption of Cr (VI). Error bars represent the standard deviations.

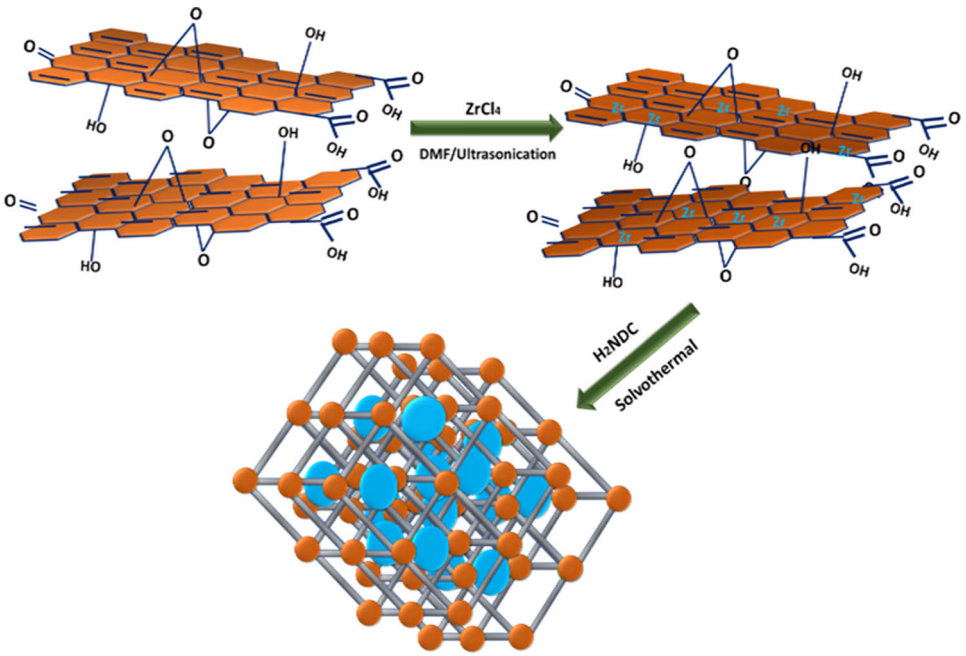

Fig. 13 | Schematic representation. Step wise procedure for the synthesis of GO/UiO-66-NDC nanocomposite.

Stainless steel autoclaves lined with Teflon were used to heat the solution mixture for 24 h at 120 °C (Fig. 13). After the solvothermal process, the substance was centrifuged for 15 min at 4500 rpm and then washed repeatedly with dimethylformamide and/or ethanol. A consistent weight was achieved by drying the finished product at 85 °C.

Material characterization

To analyze the physicochemical and structural properties of the GO/UiO-66-NDC nanocomposite, Raman, BET (Brunauer–Emmett–Teller) surface area, X-ray diffraction, UV, TGA (Thermogravimetric analysis), Scanning Electron Microscopy (SEM) with Energy Dispersive X-Ray Analysis (EDX), and IR (Infrared Spectroscopy) spectrometers were employed. GO/UiO-66-NDC nanocomposite powder was used for the Raman analysis. In back-scattering geometry, Raman spectra with a Raman shift between 100 and 1850 cm^{-1} were found using a confocal Raman spectrometer (Model -STR-300; Make-Seki Technotron Corp., Japan). A 50x objective was utilized to gather dispersed light, which was excited by a 785 nm diode laser. A 600 lines per millimeter diffraction grating was used to scatter the light, and a CCD detector was used to capture it. For all samples, 12 s exposures and 12 scans were used to record the Raman data. The fluorescent background was eliminated using GRAMS/AI data processing software. The GO/crystalline UiO-66-NDC's structure was attained using a diffractometer instrument (D8 Bruker) with a sweep rate of 4 deg/min and a range of 3° to 70° (2 values). GO/UiO-66-NDC was reduced and stabilized before and after the experiment using various functional groups, which were identified using FTIR spectra (Bruker Tensor) in ATR mode with a sweep rate of 10 kHz. Using a Perkin Elmer spectrometer (lambda 35), UV spectra between 200 and 800 nm were measured. The morphology and elemental configuration of the GO/UiO-66-NDC before and after Cr(VI) adsorption experiments were investigated using FESEM-EDX on a Zeiss ULTRA 55. X-ray

photoelectron spectroscopy (XPS) was employed to acquire the distinctive binding energies, utilizing the Thermo K-alpha instrument with an aluminum anode.

Density functional simulation

The structural relaxation of the pristine graphene oxide (GO) and the nanocomposite system was carried out through basic density functional simulations using Quantum Espresso codes[66]. The calculations were performed within the generalized gradient approximation (GGA) following the Perdew-Burke-Ernzerhof (PBE) format[67]. To account for dispersion effects, the vdW-DF scheme was applied to both systems. Lattice optimization was conducted using a $9 \times 9 \times 1$ k-point grid at 540 eV as the plane-wave cutoff energy, ensuring a force of less than 0.001 eV/Å to achieve a stable, optimized geometry. A vacuum region of 20 Å along the z-direction was maintained to minimize periodic image interactions. Moreover, the values for binding energy (E_b) of the metal atom (Cr(VI)) have been obtained in the stable structures after adsorptions. All the calculations followed with vdW dispersion correction for accurate results.

Batch adsorption studies

The synthesized GO/UiO-66-NDC nanocomposite was used to adsorb Cr(VI) from simulated wastewater at room temperature. The stock of 10 mM of Cr(VI) was prepared in a 1000 ml flask by dissolving a known quantity of $K_2Cr_2O_7$ for further experimentation. Adsorption studies were carried out in batch systems using Erlenmeyer flasks. For studying the effect of initial ion concentration, different concentrations of 10 to 50 mg L^{-1} were mixed with GO/UiO-66-NDC (50 mg) in a shaking incubator for 2 h. For optimization studies, the same experiments were carried out for pH and adsorbent dose with a change in pH and dose at constant Cr(VI) concentration. After each experimentation, solutions were filtered using Whatman No. 1 and were analyzed for the remaining concentration of Cr(VI) by ICP-MS spectroscopy. A calibration curve of R^2 more than >0.999 was prepared, using concentrations ranging from 5 to 100 ppb.

The adsorption capacity was determined by using the Eq. (8) at equilibrium:

$$q = \frac{(C_o - C)V}{m} \tag{8}$$

Where C and C_o are the final and initial concentration of Cr(VI) solution, V denotes the volume, and m represents the mass of GO/UiO-66-NDC nanocomposite.

Point of zero charge

By using the salt addition approach, the point of zero charge (PzC) of the GO/UiO-66-NDC nanocomposite was identified. 0.1 M $NaNO_3$ solutions were added to ten separate flasks, and the initial pH was adjusted from 2 to 11 using either 0.01 M NaOH or 0.01 M HCl. A 100 mL flask containing. 40 mL of each of the individual solutions were then added to 0.2 g of GO/UiO-66-NDC nanocomposite. The pH was determined using a pH meter after mixing for 24 h (PH60-Z Apera Instruments). The point of zero charges is identified by plotting the difference between the initial and final pH against the beginning pH and noting the location of the junction.

Desorption experiments

Nitric acid (0.01 M) was used to verify desorption tests on Cr(VI) from GO/UiO-66-NDC nanocomposite. The GO/UiO-66-NDC nanocomposite was previously loaded with 5 mg L^{-1} of Cr(VI), 0.5 g L^{-1} of pH 3, and 240 min of contact time. It was filtered after adsorption, and the Cr(VI) content was calculated. Using Eq. 9, the desorption rate of Cr(VI) was measured.

$$Desorption\ rate\ (\%) = \frac{Desorbed\ Cr\ (VI)}{Adsorbed\ Cr\ (VI)} \times 100 \tag{9}$$

The mean values of all the batch tests were reported after they were reproduced under the same conditions. All adsorption and desorption studies were carried out at a stirring rate of 250 rpm and a temperature of 25° C, respectively.

Data availability

The data that support the findings of this study are available from the Corresponding author upon reasonable request. Still, restrictions apply to the availability of these data, which were used under license for the current study, and so are not publicly available.

Received: 19 May 2023; Accepted: 9 February 2024;
Published online: 13 March 2024

References

1. Saravanan, A. et al. Effective water/wastewater treatment methodologies for toxic pollutants removal: processes and applications towards sustainable development. *Chemosphere* **280**, 130595 (2021).
2. Singh, S. et al. Applicability of new sustainable and efficient green metal-based nanoparticles for removal of Cr(VI): adsorption antimicrobial, and DFT studies. *Environ. Pollut.* **320**, 121105 (2023).
3. Singh, S. et al. Graphene oxide-based novel MOF nanohybrid for synergic removal of Pb (II) ions from aqueous solutions: simulation and adsorption studies. *Environ. Res.* **216**, 114750 (2023).
4. Singh, S. et al. Mechanism and kinetics of Cr(VI) adsorption on biochar derived from Citrobacter freundii under different pyrolysis temperatures. *J. Water Process Eng.* **47**, 102723 (2022).
5. Singh, S. et al. Micro (nano) plastics in wastewater: a critical review on toxicity risk assessment, behaviour, environmental impact and challenges. *Chemosphere* **290**, 133169 (2022).
6. Pavesi, T. & Moreira, J. C. Mechanisms and individuality in chromium toxicity in humans. *J. Appl. Toxicol.* **40**, 1183–1197 (2020).
7. Ponnuchamy, M. et al. Sustainable adsorbents for the removal of pesticides from water: a review. *Environ. Chem. Lett.* **1**, 3 (2021).
8. Singh, S. et al. Ecological effects, remediation, distribution, and sensing techniques of chromium. *Chemosphere* **307**, 135804 (2022).
9. Azeez, N. A., Dash, S. S., Gummadi, S. N. & Deepa, V. S. Nano-remediation of toxic heavy metal contamination: Hexavalent chromium [Cr(VI)]. *Chemosphere* **266**, 129204 (2021).
10. Ray, R. R. Adverse hematological effects of hexavalent chromium: an overview. *Interdiscip. Toxicol.* **9**, 55–65 (2016).
11. Tabatabaei, S., Forouzesh Rad, B. & Baghdadi, M. Semicontinuous enhanced electroreduction of Cr(VI) in wastewater by cathode constructed of copper rods coated with palladium nanoparticles followed by adsorption. *Chemosphere* **251**, 126309 (2020).
12. Brasili, E. et al. Remediation of hexavalent chromium contaminated water through zero-valent iron nanoparticles and effects on tomato plant growth performance. *Sci. Rep.* **10**, 1920 (2020).
13. Izzudin, N. M. et al. Simultaneous remediation of hexavalent chromium and organic pollutants in wastewater using period 4 transition metal oxide-based photocatalysts: a review. *Environ. Chem. Lett.* **19**, 4489–4517 (2021).
14. Kumar, V. & Dwivedi, S. K. A review on accessible techniques for removal of hexavalent Chromium and divalent Nickel from industrial wastewater: Recent research and future outlook. *J. Clean. Prod. vol.* **295**, 126229 (2021).
15. Sharma, N., Sodhi, K. K., Kumar, M. & Singh, D. K. Heavy metal pollution: Insights into chromium eco-toxicity and recent advancement in its remediation. *Environ. Nanotechnol. Monit. Manag* **15**, 100388 (2021).
16. Guan, X. et al. Application of functionalized layered double hydroxides for heavy metal removal: a review. *Sci. Total Environ.* **838**, 155693 (2022).
17. Khan, S. et al. Synthesis, modifications and applications of MILs Metal-organic frameworks for environmental remediation: the cutting-edge review. *Sci. Total Environ.* **810**, 152279 (2022).

18. Wang, Z. et al. Interactions between Cr(VI) and the hydrochar: the electron transfer routes, adsorption mechanisms, and the accelerating effects of wood vinegar. *Sci. Total Environ.* **863**, 160957 (2023).
19. Rajapaksha, A. U. et al. A systematic review on adsorptive removal of hexavalent chromium from aqueous solutions: recent advances. *Sci. Total Environ.* **809**, 152055 (2022).
20. Yu, S. et al. Recent advances in metal-organic framework membranes for water treatment: a review. *Sci. Total Environ.* **800**, 149662 (2021).
21. Garg, R., Gupta, R., Singh, N. & Bansal, A. Characterization and performance evaluation of synthesized ZnO nanoflowers, nanorods, and their hybrid nanocomposites with graphene oxide for degradation of Orange G. *Environ. Sci. Pollut. Res.* https://doi.org/10.1007/S11356-021-14511-3 (2021).
22. Valizadeh, B. et al. A novel integrated Cr(VI) adsorption–photoreduction system using MOF@polymer composite beads. *J. Mater. Chem. A Mater.* **8**, 9629–9637 (2020).
23. El-Mehalmey, W. A. et al. Metal–organic framework@silica as a stationary phase sorbent for rapid and cost-effective removal of hexavalent chromium. *J. Mater. Chem. A Mater.* **6**, 2742–2751 (2018).
24. Rego, R. M., Kurkuri, M. D. & Kigga, M. A comprehensive review on water remediation using UiO-66 MOFs and their derivatives. *Chemosphere* **302**, 134845 (2022).
25. Butova, V. V. et al. UiO-66 type MOFs with mixed-linkers - 1,4-Benzenedicarboxylate and 1,4-naphthalenedicarboxylate: Effect of the modulator and post-synthetic exchange. *Microporous Mesoporous Mater.* **305**, 110324 (2020).
26. Chu, J. et al. Facile and reversible digestion and regeneration of zirconium-based metal-organic frameworks. *Commun. Chem.* **3**, 1–7 (2020).
27. Wang, H. et al. Efficient and selective removal of Cr(VI) by the modified UiO-66-NH2 with phenothiazine-N-rhodanine from aqueous solution: performance and mechanisms. *Microporous Mesoporous Mater.* **336**, 111834 (2022).
28. Zhang, X., Zhang, S., Ouyang, G. & Han, R. Removal of Cr(VI) from solution using UiO-66-NH_2 prepared in a green way. *Korean J. Chem. Eng.* **39**, 1839–1849 (2022).
29. Noraee, Z., Jafari, A., Ghaderpoori, M., Kamarehie, B. & Ghaderpoury, A. Use of metal-organic framework to remove chromium (VI) from aqueous solutions 03 Chemical Sciences 0306 Physical Chemistry (incl. Structural). *J. Environ. Health Sci. Eng.* **17**, 701–709 (2019).
30. Shokouhfar, N., Aboutorabi, L. & Morsali, A. Improving the capability of UiO-66 for Cr(VI) adsorption from aqueous solutions by introducing isonicotinate N-oxide as the functional group. *Dalton Trans.* **47**, 14549–14555 (2018).
31. Rego, R. M. et al. Cerium based UiO-66 MOF as a multipollutant adsorbent for universal water purification. *J. Hazard Mater.* **416**, 125941 (2021).
32. Xie, H. et al. Cr(VI) adsorption from aqueous solution by uio-66 modified corncob. *Sustainability* **13**, 12962 (2021).
33. Wu, S. et al. Adsorption of Cr(VI) on nano Uio-66-NH2 MOFs in water. *Environ. Technol.* **39**, 1937–1948 (2018).
34. Megremi, I., Vasilatos, C., Vassilakis, E. & Economou-Eliopoulos, M. Spatial diversity of Cr distribution in soil and groundwater sites in relation with land use management in a Mediterranean region: the case of C. Evia and Assopos-Thiva Basins, Greece. *Sci. Total Environ.* **651**, 656–667 (2019).
35. Kaprara, E. et al. The use of Sn(II) oxy-hydroxides for the effective removal of Cr(VI) from water: optimization of synthesis parameters. *Sci. Total Environ.* **605–606**, 190–198 (2017).
36. Barg, S. et al. Mesoscale assembly of chemically modified graphene into complex cellular networks. *Nat. Commun.* **5**, 1–10 (2014).
37. He, Y. et al. UiO-66-NDC (1,4-naphthalenedicarboxilic acid) as a novel fluorescent probe for the selective detection of Fe3+. *J. Solid State Chem.* **285**, 121206 (2020).
38. Atzori, C. et al. Effect of benzoic acid as a modulator in the structure of UiO-66: an experimental and computational study. *J. Phys. Chem. C.* **121**, 9312–9324 (2017).
39. Butova, V. V. et al. Partial and complete substitution of the 1,4-Benzenedicarboxylate Linker in UiO-66 with 1,4-naphthalenedicarboxylate: synthesis, characterization, and H 2 -adsorption properties. *Inorg. Chem.* **58**, 1607–1620 (2019).
40. Rekha, T. N., Umadevi, M. & Rajkumar, B. J. M. Structural and spectroscopic study of adsorption of naphthalene on silver. *J. Mol. Struct.* **1079**, 155–162 (2015).
41. Butova, V. V. et al. Modulator effect in UiO-66-NDC (1, 4-naphthalenedicarboxylic acid) synthesis and comparison with UiO-67-NDC isoreticular metal-organic frameworks. *Cryst. Growth Des.* **17**, 5422–5431 (2017).
42. Garibay, S. J. & Cohen, S. M. Isoreticular synthesis and modification of frameworks with the UiO-66 topology. *Chem. Commun.* **46**, 7700–7702 (2010).
43. Scardaci, V. & Compagnini, G. Raman spectroscopy investigation of graphene oxide reduction by laser scribing. *C.* **7**, 48 (2021).
44. Singh, S. et al. A systematic study of arsenic adsorption and removal from aqueous environments using novel graphene oxide functionalized UiO-66-NDC nanocomposites. *Sci. Rep.* **12**, 1–15 (2022).
45. Cheng, M. et al. Synthesis of graphene oxide/polyacrylamide composite membranes for organic dyes/water separation in water purification. *J. Mater. Sci.* **54**, 252–264 (2019).
46. Sunil Kumar Naik, T. S. et al. Advanced experimental techniques for the sensitive detection of a toxic bisphenol A using UiO-66-NDC/GO-based electrochemical sensor. *Chemosphere* **311**, 137104 (2023).
47. Qi, H., Niu, X., Wu, H., Liu, X. & Chen, Y. Adsorption of Chromium (VI) by Cu (I)-MOF in water: optimization, Kinetics, and Thermodynamics. https://doi.org/10.1155/2021/4413095 (2021).
48. Mondal, N. K. & Chakraborty, S. Adsorption of Cr(VI) from aqueous solution on graphene oxide (GO) prepared from graphite: equilibrium, kinetic and thermodynamic studies. *Appl. Water Sci.* **10**, 61 (2020).
49. Zhou, L. et al. Efficient removal of hexavalent chromium through adsorption-reduction-adsorption pathway by iron-clay biochar composite prepared from Populus nigra. *Sep. Purif. Technol.* **285**, 120386 (2022).
50. Setshedi, K. Z., Bhaumik, M., Onyango, M. S. & Maity, A. High-performance towards Cr(VI) removal using multi-active sites of polypyrrole–graphene oxide nanocomposites: batch and column studies. *Chem. Eng. J.* **262**, 921–931 (2015).
51. Barrera-Díaz, C. E., Lugo-Lugo, V. & Bilyeu, B. A review of chemical, electrochemical and biological methods for aqueous Cr(VI) reduction. *J. Hazard Mater.* **223–224**, 1–12 (2012).
52. Di Natale, F., Erto, A., Lancia, A. & Musmarra, D. Equilibrium and dynamic study on hexavalent chromium adsorption onto activated carbon. *J. Hazard Mater.* **281**, 47–55 (2015).
53. Sarikhani, Z. & Manoochehri, M. Removal of Toxic Cr(VI) ions from water sample a novel magnetic graphene oxide nanocomposite. *Int. J. N. Chem.* **7**, 30–46 (2020).
54. Entezari A., et al. Investigation of hexavalent chromium removal from aqueous solution using granular and powdered activated carbon produced from peganum harmala seed. **15**, 645–656 (2016).
55. Mobarak, M., Selim, A. Q., Mohamed, E. A. & Seliem, M. K. A superior adsorbent of CTAB/H_2O_2 solution−modified organic carbon rich-clay for hexavalent chromium and methyl orange uptake from solutions. *J. Mol. Liq.* **259**, 384–397 (2018).
56. Zhang, L., Luo, H., Liu, P., Fang, W. & Geng, J. A novel modified graphene oxide/chitosan composite used as an adsorbent for Cr(VI) in aqueous solutions. *Int. J. Biol. Macromol.* **87**, 586–596 (2016).
57. Wang, X. et al. Facile synthesis of recycling Fe3O4/graphene adsorbents with potassium humate for Cr(VI) removal. *Col. Surf. A Physicochem. Eng. Asp.* **560**, 384–392 (2019).

58. Ren, T. et al. Synthesis of α-Fe2O3 nanofibers for applications in removal and recovery of Cr(VI) from wastewater. *Environ. Sci. Pollut. Res.* **20**, 155–162 (2013).
59. Ho, Y. S. & McKay, G. Pseudo-second order model for sorption processes. *Process Biochem.* **34**, 451–465 (1999).
60. Zhang, X. et al. Adsorption-reduction removal of Cr(VI) by tobacco petiole pyrolytic biochar: batch experiment, kinetic and mechanism studies. *Bioresour. Technol.* **268**, 149–157 (2018).
61. Rapti, S. et al. Rapid, green and inexpensive synthesis of high quality UiO-66 amino-functionalized materials with exceptional capability for removal of hexavalent chromium from industrial waste. *Inorg. Chem. Front.* **3**, 635–644 (2016).
62. Rapti, S. et al. Selective capture of hexavalent chromium from an anion-exchange column of metal organic resin–alginic acid composite. *Chem. Sci.* **7**, 2427–2436 (2016).
63. Fei, H., Bresler, M. R. & Oliver, S. R. J. A new paradigm for anion trapping in high capacity and selectivity: crystal-to-crystal transformation of cationic materials. *J. Am. Chem. Soc.* **133**, 11110–11113 (2011).
64. Singh, S. et al. Sustainable removal of Cr(VI) using graphene oxide-zinc oxide nanohybrid: Adsorption kinetics, isotherms and thermodynamics. *Environ. Res.* **203**, 111891 (2022).
65. Singh, S. et al. A novel CaO nanocomposite cross linked graphene oxide for Cr(VI) removal and sensing from wastewater. *Chemosphere* **301**, 134714 (2022).
66. Giannozzi, P. et al. QUANTUM ESPRESSO: a modular and open-source software project for quantum simulations of materials. *J. Phys.: Condens. Matter* **21**, 395502 (2009).
67. Perdew, J. P., Ernzerhof, M. & Burke, K. Rationale for mixing exact exchange with density functional approximations. *J. Chem. Phys.* **105**, 9982 (1998).

Acknowledgements

S.S. would like to acknowledge DBT HRD Project & Management Unit, Regional Center for Biotechnology, NCR Biotech Science Cluster, Faridabad, Haryana for Research Associateship (DBT-RA), funding under award letter No DBT-RA/2022/July/N/2044 dated January 12, 2023. S.K.B. would like to acknowledge UGC, Govt. of India for Dr. D. S. Kothari Postdoctoral Fellowship funding under award No.F.4–2/2006(BSR)/PH/20–21/0108, dated Sept. 14, 2021. Parts of the simulations are also performed in our server and Supercomputing facility of SERC, IISc. The authors wish to express their gratitude to the Ministry of Education (MoE) for their support under the grant MoE-STARS/STARS-2/2023-0714, dated September 26, 2023. Also would like to thank ICWaR and IISc for laboratory and instrumentation facilities.

Author contributions

Simranjeet Singh: Conceptualization, Visualization, Investigation and Writing - Original Draft; Amit G. Anil, Basavaraju U, Bidisha N, Pavithra N,: Analysis and Writing, Reviewing and Editing; Sushant K. Behera: Computational Calculations, Analysis and Writing, Shipra Bhati: Visualization and Methodology; Joginder Singh, Nadeem A. Khan: Writing, Reviewing and Editing; Praveen C. Ramamurthy: Supervision, Validation, Writing, Reviewing and Editing.

Competing interests

The authors declare no competing interests.

Ethical approval

We declare careful consideration of all the researcher contributions and authorship to promote greater equity in research collaborations.

Additional information

Supplementary information The online version contains supplementary material available at https://doi.org/10.1038/s41545-024-00306-9.

Correspondence and requests for materials should be addressed to Praveen C. Ramamurthy.